Secondary iron overload induces chronic pancreatitis and ferroptosis of acinar cells in mice

CHENYING TIAN[1], JING ZHAO[1], QINGQING XIONG[1], HONG YU[2] and HUAHUA DU[1,2]

[1]Key Laboratory of Animal Feed and Nutrition of Zhejiang Province, College of Animal Sciences, Zhejiang University, Hangzhou, Zhejiang 310058; [2]Department of General Surgery, Sir Run-Run Shaw Hospital, School of Medicine, Zhejiang University, Hangzhou, Zhejiang 310016, P.R. China

Received September 21, 2022; Accepted November 16, 2022

DOI: 10.3892/ijmm.2022.5212

Abstract. Disruption of iron homeostasis is associated with multiple diseases. It has been found that patients with genetic iron overload develop massive iron deposition in the pancreas. However, few studies have focused on the effect of secondary iron overload on the pancreas. The objective of the present study was to investigate the pathogenic consequences of secondary iron overload in mice. An iron overload mouse model was constructed by intraperitoneal injection of 120 mg/kg body weight of iron dextran every other week for 12 weeks. Iron deposition, immunocyte infiltration, fibrosis, oxidative stress and ferroptosis were assessed using Prussian blue staining, immunohistochemical analysis, Masson staining, Sirius red staining, RT-qPCR analysis and western blot analysis. It was found that iron-overloaded mice showed pancreatic iron overload, together with elevated gene expression of the iron storage factor ferritin H, and decreased expression of the iron transportation mediator divalent metal transporter 1, ferroportin 1 and transferrin receptor. Iron-overloaded mice developed mild pancreatitis with increased serum amylase and lipase activities, as well as elevated gene expression levels of pro-inflammatory cytokines, including interleukin (IL)-1β, IL-6 and inducible nitric oxide synthase. Acinar atrophy, massive immunocyte infiltration and pancreatic fibrosis were noted in the iron-overloaded mice. As an underlying mechanism, iron-overloaded mice showed increased pancreatic oxidative stress, with an elevated malondialdehyde level, and decreased SOD and glutathione peroxidase activity. Furthermore, iron overload led to ferroptosis with promoted expression of cytochrome *c* oxidase subunit II, and decreased transcripts of glutathione peroxidase 4 and solute carrier family 7 member 11. These results provided evidence that multiple intraperitoneal injections of iron dextran in mice lead to iron overload-induced chronic pancreatitis, which suggested that secondary iron overload is a risk factor for pancreatitis and highlights the importance of iron in maintaining the normal functions of the pancreas.

Correspondence to: Professor Huahua Du, Key Laboratory of Animal Feed and Nutrition of Zhejiang Province, College of Animal Sciences, Zhejiang University, 866 Yuhangtang Road, Hangzhou, Zhejiang 310058, P.R. China
E-mail: huahuadu@zju.edu.cn

Professor Hong Yu, Department of General Surgery, Sir Run-Run Shaw Hospital, School of Medicine, Zhejiang University, 3 Qingchun Road, Hangzhou, Zhejiang 310016, P.R. China
E-mail: blueyu000@zju.edu.cn

Abbreviations: HH, hereditary haemochromatosis; AP, acute pancreatitis; CP, chronic pancreatitis; MDA, malondialdehyde; SOD, superoxide dismutase; GSH-PX, glutathione peroxidase; FtH, ferritin H; DMT1, divalent metal transporter 1; FPN, ferroportin 1; TfR, transferrin receptor; IL, interleukin; α-SMA, α-smooth muscle actin; COX2, cytochrome *c* oxidase subunit II; GPX4, glutathione peroxidase 4

Key words: secondary iron overload, pancreatic iron deposition, pancreatitis, pancreatic fibrosis, ferroptosis

Introduction

Iron is one of the essential trace elements for animal organisms, and is involved in numerous life processes, such as oxygen transport (1), DNA synthesis (2), the host defense and inflammation (3). Disruption of iron homeostasis caused by iron deficiency or overload is strongly associated with some of the most common human diseases (4,5). Iron can influence the clinical course of several chronic metabolic diseases, such as type 2 diabetes (6), obesity (7), non-alcoholic fatty liver disease (8) and atherosclerosis (9).

Iron overload has been linked to a variety of human diseases, such as hereditary haemochromatosis (HH), thalassemias and neurodegeneration (10,11). Iron overload diseases result in excess body iron deposition, which can be caused by genetic or secondary causes. HH is defined as a genetically derived systemic iron overload caused by decreased concentrations of the iron regulatory hormone hepcidin or decreased hepcidin-ferroportin binding (12). Secondary iron overload may result from frequent blood transfusions, exogenous iron intake or certain haematological disorders, such as refractory anemia or aplastic anemia (13). Iron overload can cause toxic accumulation in the liver, heart, joints or endocrine glands (14). However, the clinical manifestations of iron overload syndrome are complex and far from being understood.

The pancreas is commonly affected in iron overload syndromes. Clinical data show that patients with HH are at risk of developing diabetes due to β-cell dysfunction, but may display iron overload in the pancreas (15). Significant pancreatic iron overload has been reported in other iron overload disorders, including thalassaemia, sickle cell anaemia and Diamond-Blackfan anaemia (16-18). Iron overload is also significantly associated with exocrine pancreatic dysfunction. The most common disease of exocrine pancreatic dysfunction is pancreatitis, which mainly includes acute pancreatitis (AP) and chronic pancreatitis (CP). AP is an inflammatory disease of the pancreas that is associated with high morbidity and mortality rates (19). AP is characterized by acinar cell death and local and systemic inflammation (20), whereas CP, a progressive and irreversible fibroinflammatory disease of the pancreas, consists of inflammation and pancreatic fibrosis in individuals with genetic, environmental and other risk factors (21). CP is characterized by pancreatic atrophy, fibrosis, ductal stenosis and distortion, calcification, exocrine insufficiency and diabetes mellitus (22). Pancreatitis causes alterations in circulating markers of iron in patients. In a recent study, serum iron, serum ferritin and transferrin saturation levels were all increased in patients with pancreatitis compared with those in healthy subjects, whereas these parameters were significantly decreased in patients after treatment (23). Pancreatic iron deposition has been observed in several genetic mutation models of iron overload, such as hepcidin knockout mice (24), bone morphogenetic protein-deficient mice (25) and ceruloplasmin mutants (26). However, to the best of our knowledge, there are no studies on the effect of non-hereditary iron overload on the pancreas.

Overall, iron plays a key role in life activities as an essential nutrient for body growth. Iron homeostasis plays an important role in the maintenance of pancreatic health and the development of diseases, but the specific effects and mechanisms of iron overload in the development of these pancreatic diseases are still unclear. Considering the well-established role of iron metabolism and pancreatic function in multiple transgenic mouse models, the present study aimed to further explore the pathogenic consequences of iron overload on pancreatic tissue in mice using a model of non-hereditary iron overload.

Materials and methods

Animals. A total of 20, male, 8-week-old, C57BL/6 (20±2 g) mice were purchased from Shanghai Slack Laboratory Animal Center. The mice were housed in an environment with a 12-h light/dark cycle at 24˚C and a relative humidity of 50-70%. The mice were given free access to water and food, and the bedding was changed every other day. After 7 days of acclimation, the mice were randomly divided into the following two groups with 10 mice each: Control group and iron overload group. The iron overload mice were injected intraperitoneally with 120 mg/kg body weight of iron dextran (Pharmacosmos A/S) every other week for 12 weeks. Since infused dextran is eliminated 70% by the kidney and 30% by the gastrointestinal tract, the control mice were injected intraperitoneally with saline as reported previously (27). Mice were sacrificed by cervical dislocation at the end of the experiment. The blood and pancreas were collected. Pancreas tissues were rapidly dissected and fixed in 4% paraformaldehyde solution at room temperature for 24 h for histological analysis, or frozen in liquid nitrogen and stored at -80˚C until further analysis. All animal experiments were approved by the Committee of Experimental Animal Care of Zhejiang University (Hangzhou, China; approval no. 20077).

Serum biochemical assays. Mouse serum was separated from the blood samples by centrifugation at 3,000 x g for 15 min at 4˚C. A serum iron assay kit (cat. no. A039-1-1; Nanjing Jiancheng Bioengineering Institute) and total iron binding capacity assay kit (cat. no. A040-1-1; Nanjing Jiancheng Bioengineering Institute) were used to detect the iron level of the mice according to the manufacturer's instructions. For serum iron detection, iron chromogen was added to the serum and incubated in boiling water for 5 min. After cooling and centrifugation at 3,000 x g for 10 min at 4˚C, the absorbance at 520 nm was measured by a fluorescence spectrophotometer. For measurement of total iron binding capacity, the serum was mixed with 179.1 mmol/l iron standard so that all transferrin bound iron in the serum. The excess iron in the serum was then adsorbed away using an iron adsorbent, and the iron content was measured by assessing the iron level in the serum. A lipase assay kit (cat. no. A054-2-1) and an α-amylase assay kit (cat. no. C016-1-1) (both Nanjing Jiancheng Bioengineering Institute) were used to detect amylase and lipase levels, respectively, in the mouse serum. α-amylase hydrolyzes the starch in the substrate. In the case of known substrate concentration and excess, the added iodine solution can combine with the unhydrolyzed starch in the substrate to form a blue complex. The absorbance at 660 nm was measured by a fluorescence spectrophotometer to obtain the amount of starch that had been hydrolyzed, and thus the activity of α-amylase was calculated. Latex made of triglyceride and water has a turbid character due to the absorption and scattering of incident light by its micelles. The triglycerides in the micelles are hydrolyzed by the action of lipase, which causes the micelles to split and thus the scattered light or turbidity is reduced. Lipase activity was calculated by measuring the absorbance at 420 nm using fluorescence spectrophotometer and measuring the rate of reduction of scattered light or turbidity.

Histological analysis. Paraffin-embedded samples were cut into 5-μm sections. For haematoxylin and eosin (H&E) staining, paraffin sections were deparaffinized with xylene and rehydrated using different concentrations of alcohol, and then stained with haematoxylin for 5 min. The sections were differentiated in aqueous hydrochloric acid for 2 sec and blunted in aqueous ammonia for 15-30 sec at room temperature. The sections were put into eosin staining solution for 5-8 sec at room temperature. The sections were mounted with neutral gum after dehydration using absolute ethanol and xylene. The H&E staining then examined by light microscope (Leica Microsystems GmbH) and image acquisition was performed to analyze the histopathological features of the pancreatic sections.

Prussian blue staining was used to detect iron deposition in the pancreatic tissues. The 5-μm sections of pancreas were deparaffinized with xylene and rehydrated using different concentrations of alcohol. Pancreatic tissue was incubated in a mixture (1:1) of 2% potassium ferrocyanide and 2%

hydrochloric acid for 30 min at room temperature. Sections were then rinsed with PBS (cat. no. KGB5001; Nanjing KeyGen Biotech Co., Ltd.) and counterstained with eosin for 20 sec at room temperature. The sections were mounted with neutral gum after dehydration using absolute ethanol and xylene.

Masson staining and Sirius red staining were employed to evaluate the collagen content of the pancreas. For Masson staining, paraffin sections were deparaffinized with xylene and rehydrated using different concentrations of alcohol. The sections were then placed in potassium dichromate standards at room temperature overnight (~17 h). Sections were treated with aqueous phosphomolybdic acid for 1-2 min and counterstained with aniline blue liquid for 5 sec at room temperature. Sections were sequentially treated with 1% glacial acetic acid for 5-10 sec each at room temperature. Sections were dehydrated and mounted using neutral resin glue. For Sirius red staining, pancreatic tissue sections were deparaffinized and stained with Wiegert's iron haematoxylin stain for 15 min at room temperature. Next, pancreatic sections were differentiated with an acidic differentiation solution. After washing the sections in tap water for 10 min, the pancreatic tissue was stained with Sirius red staining droplets for 1 h at room temperature. The sections were gently rinsed with a flowing water stream to remove the surface dye solution. All sections were examined using a DM3000 microscope (Leica Microsystems GmbH). The inflammation, atrophy and fibrosis in the pancreatic tissues were scored from 0 to 3 using a histopathological scoring criteria system, as previously reported (28).

Immunohistochemical analysis. The pancreatic sections were deparaffinized in xylene and then sequentially dehydrated in different concentrations of ethanol solution. Endogenous peroxidase activity was blocked with 3% H_2O_2 for 10 min, and sections were resuspended in antigen retrieval solution (pH 6.0) and boiled in a microwave oven for 5 min. Pancreatic tissue was then blocked with 3% bovine albumin [cat. no. 36101ES25; Yeasen Biotechnology (Shanghai) Co., Ltd.]. for 1 h at room temperature. Sections were incubated overnight at 4˚C with anti-CD11b antibody (1:1,000; cat. no. ab133357), anti-F4/80 antibody (1:5,000; cat. no. ab300421) and anti-CD3 antibody (1:150; cat. no. ab16669) antibodies (all Abcam), then washed with Tris-buffered saline containing 0.1% Tween-20 (TBST). The pancreatic tissues were incubated with anti-rabbit IgG H&L (conjugated with horseradish peroxidase; 1:5,000 cat. no. ab205718; Abcam) for 1 h at room temperature, and then stained and developed with horseradish peroxidase for 30 min. Finally, the nuclei were counterstained using haematoxylin solution for 30 sec at room temperature. All sections were examined using a DM3000 microscope (Leica Microsystems GmbH). In this experiment, immunohistochemical quantification was performed using ImageJ software (version 2.0; National Institutes of Health).

Determination of pancreatic malondialdehyde (MDA) content, and superoxide dismutase (SOD) and glutathione peroxidase (GSH-PX) activity. The levels of MDA, SOD and GSH-PX in the pancreatic tissues were measured by MDA (cat. no. A003-1-1), SOD (cat. no. A001-1-1) and GSH-PX (cat. no. A005-1-2) assay kits (Nanjing Jiancheng Bioengineering Institute), respectively, according to the manufacturer's instructions. MDA can combine with thiobarbituric acid to form a red product with an absorption maximum at 532 nm using a fluorescence spectrophotometer. SOD generates superoxide anion radical (O_2^-) through xanthine and the xanthine oxidase reaction system, which oxidizes hydroxylamine to form nitrite, presenting a purple red color under the action of chromogenic agents. Therefore, the activity of SOD can be determined by measuring the absorbance at 550 nm using a fluorescence spectrophotometer. GSH-PX can promote the reaction of hydrogen peroxide (H_2O_2) with reduced GSH to produce H_2O and the oxidized GSH. The activity of GSH-PX can be expressed as the rate of its enzymatic reaction. GSH and dithiodinitrobenzoic acid act to generate 5-thiodinitrobenzoate anions exhibiting a more stable yellow color, and the amount of GSH can be calculated by measuring its absorbance at 412 nm using a fluorescence spectrophotometer.

Analysis by reverse transcription-quantitative polymerase chain reaction (RT-qPCR). Total RNA from the pancreas was extracted using Total RNA Extraction Reagent (cat. no. BS259A; Biosharp Life Sciences) and reverse-transcribed into cDNA using Hifair® III 1st Strand cDNA Synthesis SuperMix for qPCR [cat. no. 11141ES60; Yeasen Biotechnology (Shanghai) Co., Ltd.] according to the manufacturer's protocols. The concentration of RNA was determined using a Nanodrop 2000 spectrophotometer (Thermo Fisher Scientific, Inc.). Real-time qPCR was performed using Hief UNICON® qPCR SYBR Green Master Mix [cat. no. 11200ES08; Yeasen Biotechnology (Shanghai) Co., Ltd.] and the ABI 7500 Real-Time PCR system (Thermo Fisher Scientific, Inc.). The following thermocycling conditions were used for the qPCR: Initial denaturation at 95˚C for 1 min; followed by 40 cycles at 95˚C for 15 sec and 60˚C for 1 min. The fold difference in gene expression was calculated using the $2^{-\Delta\Delta Cq}$ method and presented relative to endogenous β-actin mRNA (29). All reactions were performed at least in triplicate. Primer sequences are listed in Table I.

Western blot analysis. Total pancreatic protein was isolated using Cell Lysis Buffer for Western and IP (cat. no. BL509A; Biosharp Life Sciences). The total protein concentration was measured by BCA Protein Assay kit (cat. no. KGP902; Nanjing KeyGen Biotech Co., Ltd.). Protein samples (25 μg/lane) were separated on 10% gels using SDS-PAGE, and then transferred to PVDF membranes. At room temperature, the membranes were blocked with 5% skimmed milk for 1 h. The membranes were incubated overnight with the following primary antibodies at 4˚C: β-actin (1:10,000; cat. no. ET1702-52; HuaBio); glutathione peroxidase 4 (GPX4; 1:1,000; cat. no. ER1803-15; HuaBio), SLC7a11 (1:1,000; cat. no. HA600097; HuaBio) and cytochrome *c* oxidase subunit II (COX2; 1:1,000; cat. no. 4842S; Cell Signaling Technology, Inc.). Next, the membranes were incubated with HRP-linked goat anti-rabbit IgG (1:5,000; cat. no. BL003A; Biosharp Life Sciences) at room temperature for 1 h. The target proteins in the membranes were visualized by enhanced chemiluminescence detection kit (cat. no. BL520A; Biosharp Life Sciences). The band strength was analyzed using ImageJ software (version 2.0; National Institutes of Health) and normalized to β-actin protein intensity.

Table I. Primers used in quantitative polymerase chain reaction.

Gene	Primers (5'-3')	Accession number
IL-1β	F: AGTTGACGGACCCCAAAAG	NM_008361.4
	R: TTTGAAGCTGGATGCTCTCAT	
IL-6	F: CCCCAATTTCCAATGCTCTCC	NM_031168.2
	R: CGCACTAGGTTTGCCGAGT	
iNOS	F: CTCACCTACTTCCTGGACATTAC	NM_010927.4
	R: CAATCTCTGCCTATCCGTCTC	
IL-10	F: GCTCTTACTGACTGGCATGAG	NM_010548.2
	R: CGCAGCTCTAGGAGCATGTG	
FtH	F: TGGAACTGCACAAACTGGCTACT	NM_010239.2
	R: ATGGATTTCACCTGTTCACTCAGATAA	
Fpn	F: ATGGGAACTGTGGCCTTCAC	NM_016917.2
	R: TCCAGGCATGAATACGGAGA	
DMT1	F: TCTGGGCAGTGGGGATCCTG	NM_001146161.1
	R: GACGAGCAGGGTGGGGATGA	
TfR	F: TCGTACAGCAGCGGAAGT	NM_001357298.1
	R: TCTCCACGAGCGGAATACAG	
COX2	F: CCTCGTCCAGATGCTA	NM_011198.4
	R: CTCGGCTTCCAGTATTG	
GPX4	F: CGCGATGATTGGCGCT	NM_001037741.4
	R: CACACGAAACCCCTGTACTTATCC	
SLC7A11	F: TGGCGGTGACCTTCTCTGA	NM_011990.2
	R: ACAAAGATCGGGACTGCTAATGA	
Sox9	F: CACACGTCAAGCGACCCATGAA	NM_011448.4
	R: TCTTCTCGCTCTCGTTCAGCAG	
Krt19	F: AATGGCGAGCTGGAGGTGAAGA	NM_001313963.1
	R: CTTGGAGTTGTCAATGGTGGCAC	
Vim	F: CGGAAAGTGGAATCCTTGCAGG	NM_011701.4
	R: AGCAGTGAGGTCAGGCTTGGAA	
CD3e	F: ATGCGGTGGAACACTTTCTGG	NM_007648.5
	R: GCACGTCAACTCTACACTGGT	
CD11b	F: CCATGACCTTCCAAGAGAATGC	NM_001082960.1
	R: ACCGGCTTGTGCTGTAGTC	
Mrc1	F: CTCTGTTCAGCTATTGGACGC	NM_008625.2
	R: TGGCACTCCCAAACATAATTTGA	
α-SMA	F: GTCCCAGACATCAGGGAGTAA	NM_007392.3
	R: TCGGATACTTCAGCGTCAGGA	
Col1a1	F: GCTCCTCTTAGGGGCCACT	NM_007742.4
	R: CCACGTCTCACCATTGGGG	
CTGF	F: CAGAGTGGAGCGCCTGTT	NM_010217.2
	R: GGATGCACTTTTTGCCCTTCT	
Fibronectin-1	F: CGAAGAGCCCTTACAGTTCC	NM_001276408.1
	R: CCGTGTAAGGGTCAAAGCAT	
β-actin	F: CCACCATGTACCCAGGCATT	NM_007393.5
	R: AGGGTGTAAAACGCAGCTCA	

FtH, ferritin H; DMT1, divalent metal transporter 1; FPN, ferroportin 1; TfR, transferrin receptor; COX2, cytochrome *c* oxidase subunit II; GPX4, glutathione peroxidase 4; SCL7A11, solute carrier family 7 member 11; IL, interleukin; iNOS, inducible nitric oxide synthase; Sox9, SRY-related high-mobility-group-box gene 9; Krt19, keratin 19; Vim, vimentin; Mrc1, mannose receptor C type 1; α-SMA, α-smooth muscle actin; Col1a1, collagen type I α1; CTGF, connective tissue growth factor.

Statistical analysis. Results are shown as the mean ± standard error of the mean. Statistical analysis was performed using GraphPad Prism 8.0 software (GraphPad Software, Inc.). Differences between the two groups were compared using an

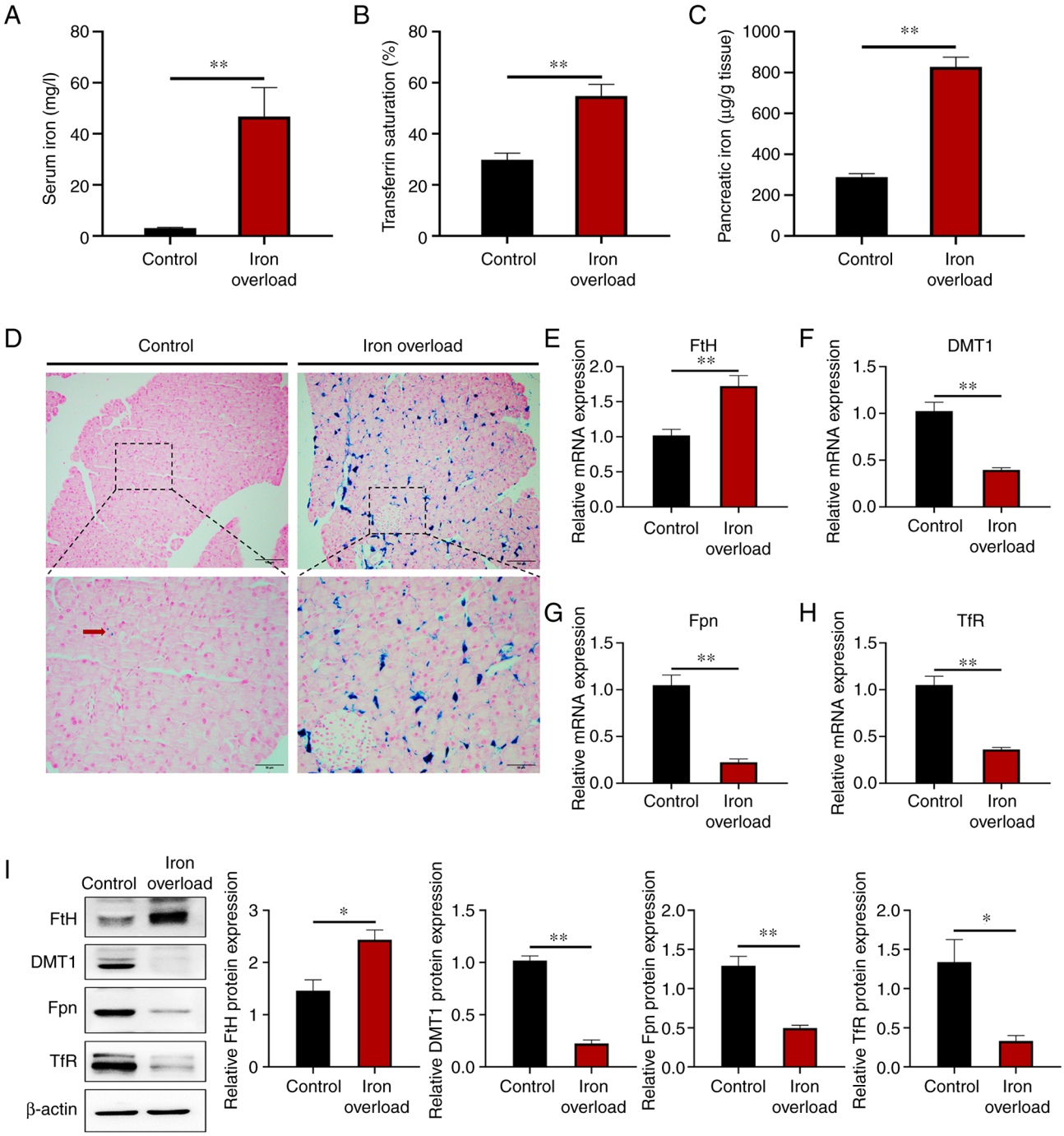

Figure 1. Iron-overloaded mice have massive iron deposition in the pancreas. Male, 8-week-old, C57BL/6 mice were injected intraperitoneally with 120 mg/kg body weight of iron dextran every other week for 12 weeks. (A) Iron content in the serum. (B) Transferrin saturation in the serum. (C) Pancreatic iron content. (D) Prussian blue staining in the pancreas. Scale bars: Upper, 100 μm; lower, 50 μm. (E-H) Relative gene expression of (E) *FtH*, (F) *DMT1*, (G) *FPN* and (H) *TfR* in pancreatic tissue. (I) FtH, DMT1, Fpn and TfR protein expression levels were detected by western blotting in the pancreas. Values are expressed as the mean ± standard error of the mean. Differences between the two groups were compared using an unpaired two-tailed Student's t-test. *P<0.05; **P<0.01 (n=6 per group). FtH, ferritin H; DMT1, divalent metal transporter 1; FPN, ferroportin 1; TfR, transferrin receptor.

unpaired two-tailed Student's t-test. P<0.05 was considered to indicate a statistically significant difference.

Results

Iron-overloaded mice have massive iron deposition in the pancreas. The iron overload mouse model was constructed by intraperitoneal injection of 120 mg/kg body weight of iron dextran every other week for 12 weeks. Serum iron, transferrin saturation and pancreatic tissue iron levels were all significantly (P<0.01) elevated in the mice with iron dextran injection (Fig. 1A-C). Prussian blue staining revealed a large number of Prussian blue-positive spots, hemosiderin, in the pancreas of the mice injected with iron dextran (Fig. 1D). Massive iron deposition was showed in the exocrine rather than the endocrine pancreas. Moreover, the mRNA level of iron storing protein ferritin H (*FtH*) was significantly (P<0.01) increased in the pancreas of iron-treated mice, while those

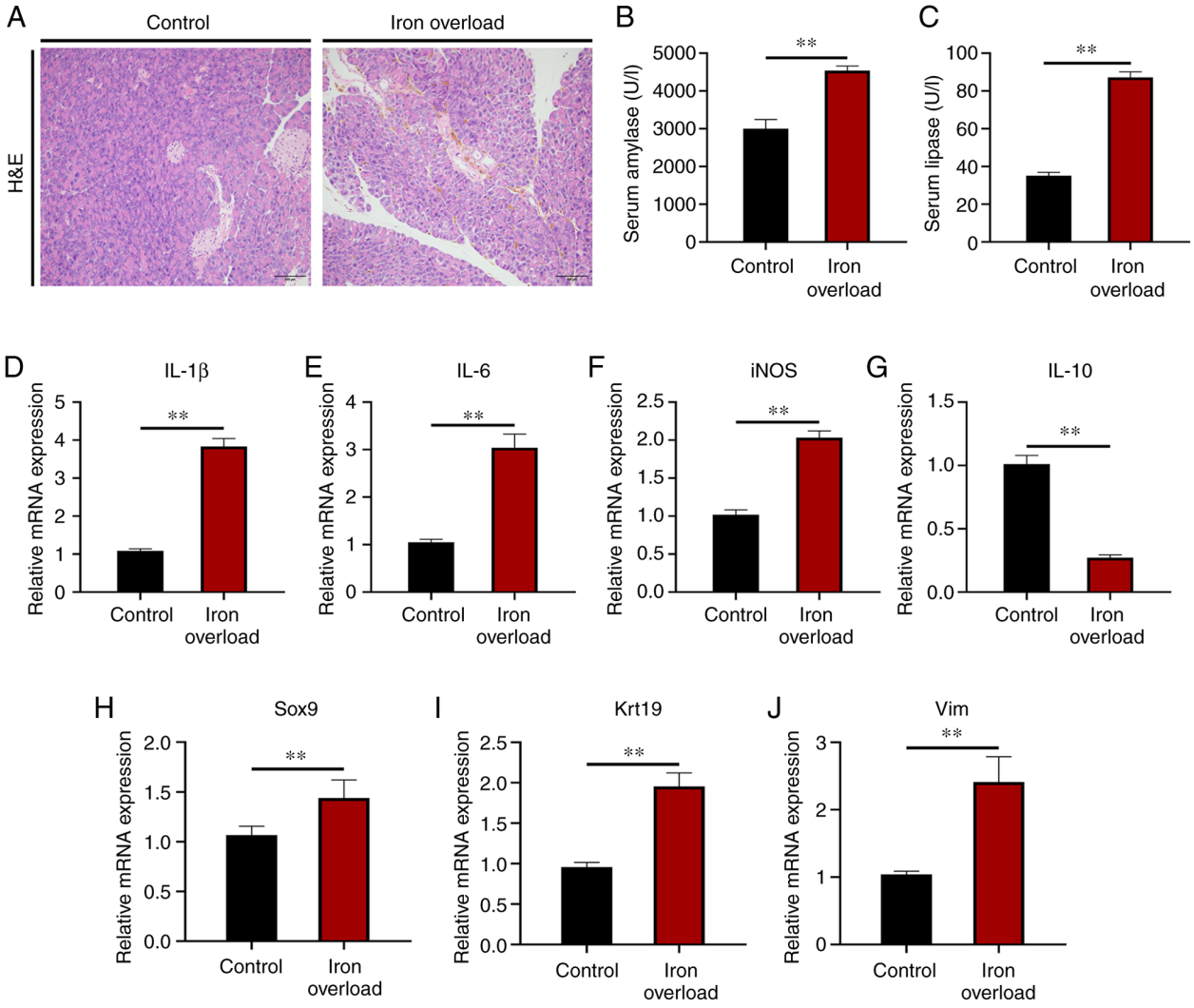

Figure 2. Iron-overloaded mice develop mild chronic pancreatitis. (A) Haematoxylin and eosin staining in the pancreas. Scale bar, 100 μm. (B) Amylase level in the serum. (C) Lipase level in the serum. (D-G) Relative gene expression of inflammatory cytokines including (D) *IL-1β*, (E) *IL-6*, (F) *iNOS* and (G) *IL-10* in pancreatic tissue. (H-J) Relative gene expression of pancreatic injury markers (H) *Sox9*, (I) *Krt19* and (J) *Vim* in the pancreas. Values are expressed as the mean ± standard error of the mean. Differences between the two groups were compared by an unpaired two-tailed Student's t-test. **P<0.01 (n=6 per group). IL, interleukin; iNOS, inducible nitric oxide synthase; Sox9, SRY-related high-mobility-group-box gene 9; Krt19, keratin 19; Vim, vimentin.

of iron transporting membrane proteins divalent metal transporter 1 (*DMT1*), ferroportin 1 (*FPN*) and transferrin receptor *(TfR)* were all significantly (P<0.01) decreased (Fig. 1E-H). The protein level of iron storing protein FtH was significantly (P<0.05) increased in the pancreas of iron-treated mice, while those of iron transporting membrane proteins DMT1, FPN, and iron binding receptor TfR were all significantly (P<0.05) decreased (Fig. 1I). The results indicated that the iron overload mouse model was successfully established and that large amounts of iron were deposited in the pancreas.

Iron-overloaded mice develop mild chronic pancreatitis. In view of the obvious pancreatic iron deposition in iron-overloaded mice, the effect of iron overload on the morphology and function of the pancreas was then analyzed. H&E staining showed that the acinar cells of the pancreas in iron-overloaded mice were atrophied and the area of intercellular substance was larger compared with those of control mice (Fig. 2A), which suggested mild pancreatic injury existed in the iron-overloaded mice. Serum amylase and lipase activities were both significantly (P<0.01) increased in the iron-overloaded mice compared with those of the control mice (Fig. 2B and C). Moreover, compared with those of the control group, the mRNA expression levels of pro-inflammatory cytokines, including interleukin (*IL*)*-1β*, *IL-6* and inducible nitric oxide synthase, were significantly (P<0.01) increased in the pancreas of iron-overloaded animals (Fig. 2D-F). Accordingly, the transcript of anti-inflammatory cytokine *IL-10* was significantly (P<0.01) decreased in the pancreas of iron-overloaded mice (Fig. 2G). Furthermore, the mRNA levels of SRY-related high-mobility-group-box gene 9 (a molecular marker of acinar to ductal metaplasia), keratin 19 (a molecular marker of ductal lesions) and vimentin (a molecular marker of stromal response) were all significantly (P<0.01) elevated by iron injection (Fig. 2H-J). The results indicated that iron overload induced mild CP and resulted in pancreatic injury.

Iron-overloaded mice show increased immunocyte infiltration in the pancreas. Histological evaluation of the pancreatic

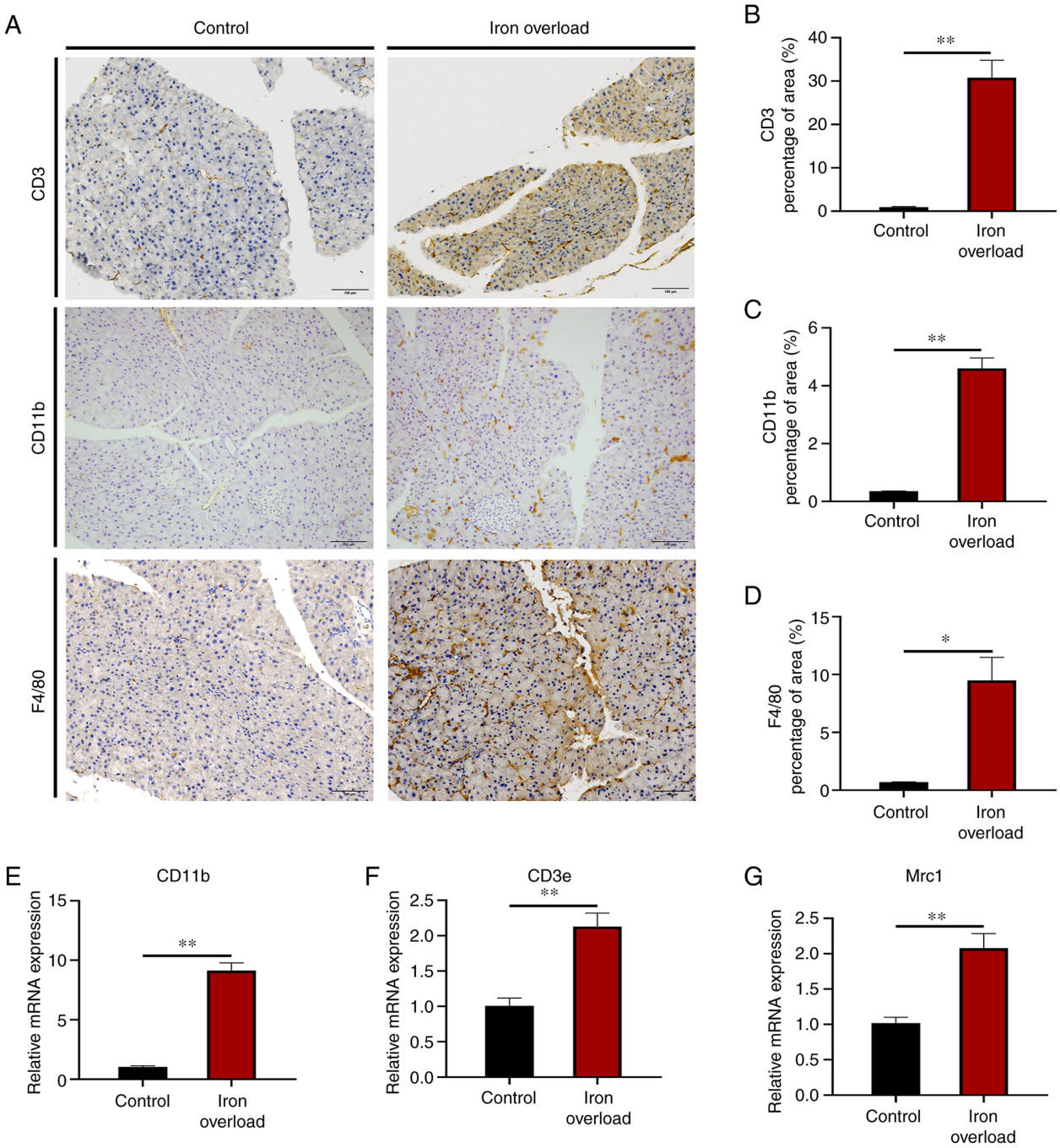

Figure 3. Iron-overloaded mice show increased immunocyte infiltration in the pancreas. (A) Representative images of the infiltration of CD3 (lymphocyte marker), CD11b (neutrophil marker) and F4/80 (macrophage marker) in the pancreas, Scale bar, 100 μm. (B-D) The quantification of positive cells of (B) CD3, (C) CD11b and (D) F4/80 in three random fields of view/each pancreatic section. (E-G) Relative gene expression of (E) *CD11b*, (F) *CD3e* and (G) *Mrc1* in the pancreas. Values are expressed as the mean ± standard error of the mean. Differences between the two groups were compared by an unpaired two-tailed Student's t-test. *P<0.05; **P<0.01 (n=6 per group). Mrc1, mannose receptor C type 1.

lesions showed that increased levels of lymphocytes (anti-CD3), neutrophils (anti-CD11b) and macrophages (anti-F4/80) were observed in the pancreas of iron-overloaded mice compared with those of control mice (Fig. 3A). The quantitative positive areas of CD3 (P<0.01), CD11b (P<0.01) and F4/80 (P<0.05) cells showed a significant increase in the pancreas of the iron-overloaded mice compared with those in the control mice (Fig. 3B-D). Furthermore, the mRNA expression of *CD11b*, *CD3e* (lymphocyte marker) and mannose receptor C type 1 (macrophage marker) was significantly (P<0.01) increased relative to the control group (Fig. 3E-G). The results indicated that pancreatic accumulation of immunocytes, including lymphocytes, neutrophils and macrophages, was present in iron-overloaded mice, which was characteristic of CP.

Iron-overloaded mice display pancreatic fibrosis. Since pancreatitis symptoms were shown in the iron-overloaded mice, Masson's trichrome and Sirius red staining were next performed to assess collagen accumulation in the pancreatic tissue sections to examine the degree of pancreatic fibrosis. The

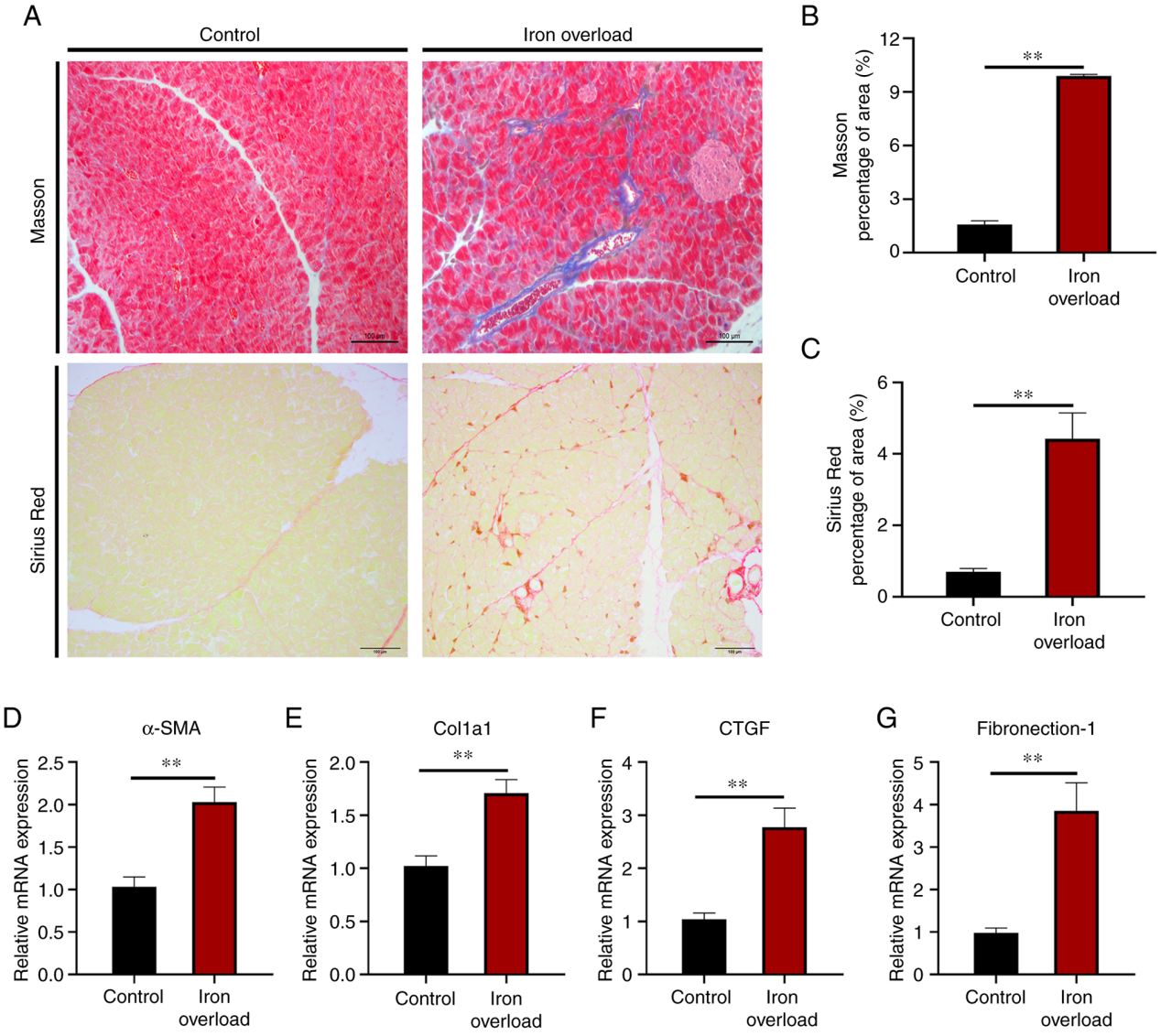

Figure 4. Iron-overloaded mice display pancreatic fibrosis. (A) Masson and Sirius Red staining in the pancreas. Scale bar, 100 μm. (B and C) The histological fibrosis quantification of (B) Masson and (C) Sirius Red staining. (D-G) Relative gene expression of pancreatic fibrosis markers, including (D) *α-SMA*, (E) *Col1a1*, (F) *CTGF* and (G) fibronection-1 in the pancreas. Values are expressed as the mean ± standard error of the mean. Differences between the two groups were compared by an unpaired two-tailed Student's t-test. **P<0.01 (n=6 per group). α-SMA, α-smooth muscle actin; Col1a1, collagen type I α1; CTGF, connective tissue growth factor.

analysis showed that iron overload induced perivascular collagen accumulation (Fig. 4A). Semi-quantitative morphometric analysis demonstrated that the collagen-positive area of tissue sections was significantly (P<0.01) increased in the pancreas of iron-overloaded mice compared with that of the control group (Fig. 4B and C). Additionally, analysis of transcripts of pancreatic fibrosis markers, such as α-smooth muscle actin (*α-SMA*), collagen type I α1, connective tissue growth factor and fibronectin-1, showed a significant (P<0.01) increase in their levels in the pancreas tissue of iron-overloaded mice (Fig. 4D-G). It was observed that the development of atrophy, inflammatory cell infiltration and fibrosis in the pancreatic tissue of iron-overloaded mice was significantly higher than that of control mice. Statistical comparisons between groups are summarized in Table II.

Iron-overloaded mice exhibit increased oxidative stress and ferroptosis in the pancreas. Oxidative stress is a common pathogenesis of a number of chronic diseases, and it is well known that iron overload affects the redox state. Compared with that of the control group, the MDA level was increased by 1.12-fold (P<0.01) in the pancreas of iron-overloaded mice (Fig. 5A). However, the injection of iron dextran led to a reduction of SOD activity by 52% (P<0.01) and GSH-PX activity by 37% (P<0.01) in the pancreas (Fig. 5B and C). This suggested that excess iron could elevate the pancreatic oxidative stress of pancreatic acinar cells in mice. Moreover, the injection of iron dextran significantly (P<0.05) promoted COX2 (a putative molecular marker of ferroptosis) protein expression, but inhibited GPX4 and SLC7A11 protein expression in the pancreas of iron-overloaded mice compared with the control group (Fig. 5D). The mRNA level of *COX2* was also significantly (P<0.01) increased, and *GPX4* and *SLC7A11* were significantly (P<0.01) decreased in the pancreas of iron-overloaded mice compared with the levels in control

Table II. Comparison of mean histopathological scores of the groups (n=5).

	Groups	
Histopathological score	Control	Iron overload
0, n (%)	3 (60)	-
1, n (%)	2 (40)	-
2, n (%)	-	1 (20)
3, n (%)	-	1 (20)
4, n (%)	-	1 (20)
5, n (%)	-	1 (20)
6, n (%)	-	1 (20)
Mean ± SEM	0.4±0.490	4±1.414
P-value (iron overload)		0.0013

SEM, standard error of the mean.

mice (Fig. 5E-G). The results indicated that iron overload induced ferroptosis.

Discussion

Genetic mutant mouse models, such as hepcidin knockout mice and BMP6 knockout mice, were previously found to have a large amount of iron deposition in the pancreas, while diet-induced iron overload did not lead to iron accumulation in the pancreas (24,25). The present study identified that the long-term injection of iron dextran caused iron overload in the mouse pancreas and induced CP. The injection animal model was adopted instead of the knockout model and the oral animal model. Although it could not better reveal the pathogenesis of iron overload syndrome, it could simulate the phenomenon of iron overload caused by disease-dependent blood transfusion and explore the influence of acquired iron overload on the development of pancreatic diseases.

Iron dextran, currently one of the most widely used iron preparations in livestock production, has previously been used to establish an iron overload mouse model by intraperitoneal injection with concentrations of 100-300 mg/kg (30,31). We previously established an iron overload mouse model by injecting 120 mg/kg of iron dextran intraperitoneally every other week for 12 weeks. A large amount of iron deposition was found, as well as obvious lipid peroxidation and ferroptosis in the liver of iron overload mice, and the iron metabolism of the body was seriously unbalanced (30). In the present study, intraperitoneal injection of iron dextran resulted in circulatory iron overload with significantly increased serum iron and transferrin saturation, and iron accumulation in the pancreatic tissues of the mice. Gene expression of iron transporting proteins such as DMT1, fpn1 and TfR1 was significantly reduced, whereas levels of iron storing proteins such as FtH were significantly elevated in the pancreas, which was similar to the results for intestinal iron overload (32). Previous studies demonstrated that iron accumulation was mainly observed in exocrine pancreatic acini in hepcidin knockout mice and Bmp6 knockout mice, but not in pancreatic islets. Thus, iron deposition in both congenital and acquired iron overload occurs at the same location, in the acini of the exocrine glands of the pancreas (24,25). These results suggested that the present non-hereditary iron overload model of mice was successfully established, and massive iron deposition was observed in the pancreas.

Previous studies have found that iron overload can lead to the atrophy and dysfunction of organs such as the liver, heart, muscles or brain (33,34). In the present study, iron accumulation in the pancreas may be associated with pancreatic dysfunction. The most common disease of the pancreatic exocrine disorders is pancreatitis, which mainly includes CP and AP. Clinically, CP continuously damages pancreatic endocrine and exocrine tissues due to repeated episodes of AP and chronic inflammation (35). In the later stage of CP, pain, sclerosis, calcification, diabetes and/or lipo-dysentery are manifested (36). The pathological features of CP are diverse, and the most common include acinar atrophy, immune infiltration, fibrosis, ductal irregularity, stenosis and dilatation (37). Hepcidin knockout mice at 6 and 12 months of age were found to exhibit a significantly increased serum lipase level, a reduced pancreatic acinar cell content and a large amount of macrophage infiltration compared with control mice and iron-rich diet mice (24). The present study demonstrated that iron overload damaged pancreatic acinar cells, enlarged intercellular spaces and caused pancreatic ductal lesions. The pancreases of iron-overloaded mice secreted large amounts of amylase and lipase into the blood, and produced a large number of pro-inflammatory factors. Therefore, mild CP was present in the pancreas of iron-overloaded mice. Since mild CP was found in the mice with iron overload during the late sample detection, a positive control group was not set up in the early experimental design. In addition, CP is regulated by the release of a variety of proinflammatory and anti-inflammatory cytokines and chemokines (38). At the same time, these inflammatory signals recruit granulocytes (neutrophils and eosinophils), monocytes, macrophages and lymphocytes to regulate the development of CP (39).

Neutrophils are traditionally considered as the first line of defense against foreign microorganisms in the innate immune system, with limited proinflammatory functions (40). Although there is less infiltration of neutrophils than macrophages in the development of CP, they are associated with disease progression and disease symptoms in CP (41). Neutrophils can activate the secretion of inflammatory cytokines by various immune cells and stromal cells, leading to the aggravation of inflammation (42). Unlike classical activation of macrophages (M1) during AP, it has been shown that M2-like macrophages predominate in CP (39). GPX4 knockout (a mouse model of ferroptosis) promoted macrophage infiltration and activation (43). The present results confirmed that iron overload promoted the infiltration of neutrophils in the pancreas of mice, and then increased the inflammatory response of the pancreas. Although neutrophils and monocytes/macrophages have been recognized as the main acting leukocyte populations of the inflamed pancreas, a local imbalance of T cells at the site of inflammation and in the circulation has also been observed in

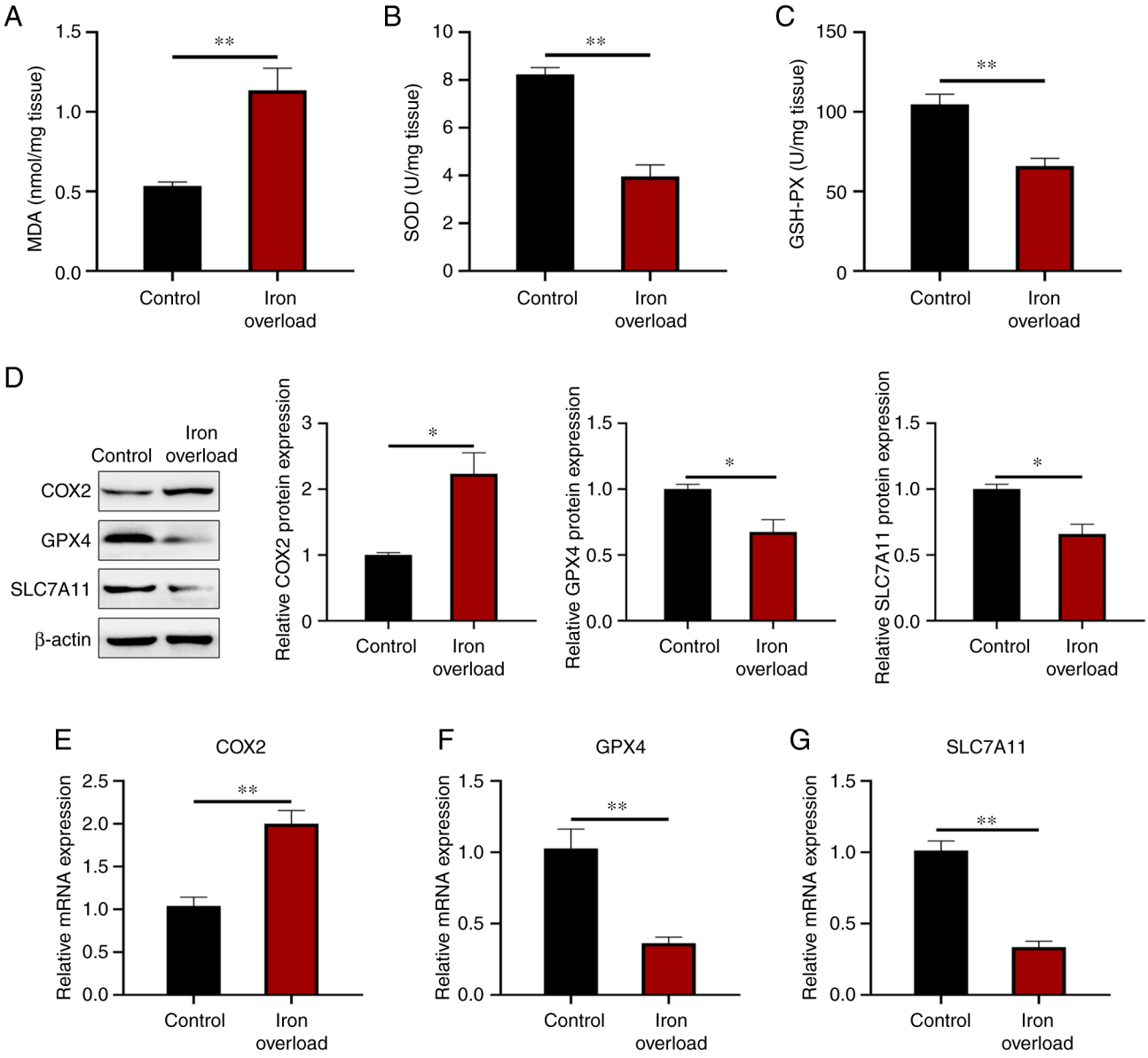

Figure 5. Iron-overloaded mice exhibit increased oxidative stress and ferroptosis in the pancreas. (A) MDA content, and (B) SOD and (C) GSH-PX activity in the pancreas. (D) COX2, GPX4 and SLC7A11 protein expression levels were detected by western blotting in the pancreas. (E-G) Relative gene expression of pancreatic fibrosis markers, including (E) *COX2*, (F) *GPX4* and (G) *SLC7A11* in the pancreas. Values are expressed as the mean ± standard error of the mean. Differences between the two groups were compared by an unpaired two-tailed Student's t-test. *P<0.05; **P<0.01 (n=6 per group). MDA, malondialdehyde; SOD, superoxide dismutase; GSH-PX, glutathione peroxidase; COX2, cytochrome *c* oxidase subunit II; GPX4, glutathione peroxidase 4; SCL7A11, solute carrier family 7 member 11.

pancreatitis (39). A study showed that massive infiltration of mouse pancreatic neutrophils and macrophages in hepcidin knockout mice induced pancreatitis, whereas $CD3^+$ T cells showed little change (24). In contrast with this, in the present study, iron-overloaded mice showed increased infiltration of $CD3^+$ T cells, macrophages and neutrophils.

Cytokines and chemokines induced by immune cells can activate pancreatic stellate cells and accelerate disease progression (38). Pancreatic stellate cells are the major contributing cells in the progression of pancreatic fibrosis (44). Pancreatic fibrosis is one of the important hallmarks of pancreatitis and pancreatic cancer (45). One study demonstrated that aging Bmp6 knockout mice developed pancreatic fibrosis with collagen distributed in the interlobular, periacinar and peripancreatic ducts (25). The present results showed that iron overload promoted the progression of pancreatic fibrosis in mice. Studies have confirmed that activated pancreatic stellate cells (α-SMA-positive cells) can promote pancreatic fibrosis by secreting extracellular matrix components, such as collagen and fibronectin, during the progression of pancreatic fibrosis (46). In the present study, the expression of α-SMA, collagen and fibronectin was increased in the pancreases of iron-overloaded mice. These results indicated that iron overload could activate pancreatic stellate cells and promote the progression of pancreatitis.

Iron overload can generate reactive oxygen species, leading to dysfunction of mitochondria and other organelles, lipid peroxidation, cell damage and death (47). Ferroptosis, an iron-dependent non-apoptotic regulated form of cell death, exhibits unique features that distinguish it from other types

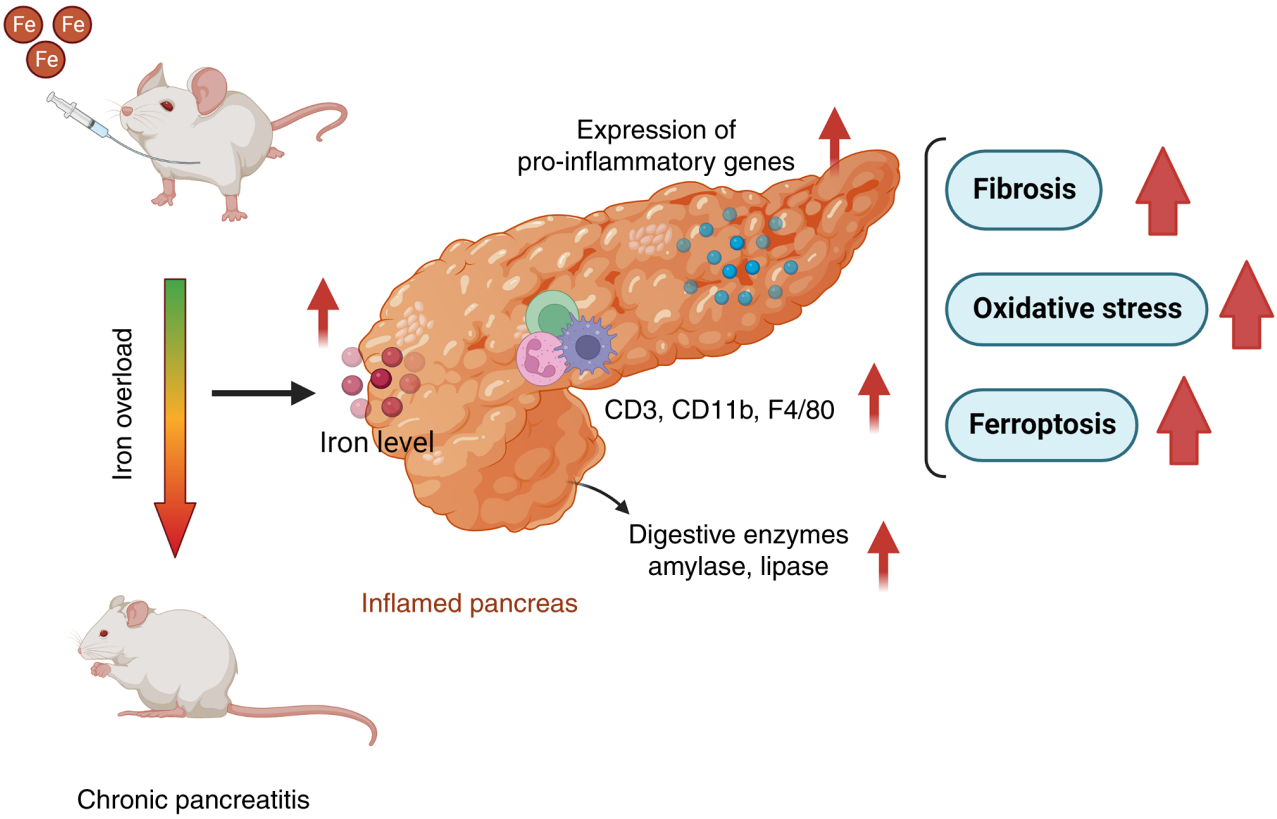

Figure 6. Secondary iron overload induced by multiple intraperitoneal injections of iron dextran results in chronic pancreatitis in mice. The schemata was created with BioRender.com.

of cell death such as apoptosis, autophagy and necrosis (48). Ferroptosis has two major typical features, namely, the accumulation of Fe^{2+} and an increase in lipid peroxidation (49). Increased peroxides are usually characterized by increased MDA content, accompanied by changes in markers of ferroptosis such as SLC7A11, GPX4 and COX2. When iron overload causes oxidative stress, it will lead to changes in MDA content, and SOD and GSH-PX enzyme activity (50). MDA is one of the end products of the lipid peroxidation of polyunsaturated fatty acids (51), which can be produced by either enzymatic pathways or non-enzymatic processes (52). MDA is not only a biomarker of oxidative stress, but also a bioactive compound with multiple biological effects (53). SOD is an antioxidant defense enzyme that plays a crucial role in the balance between theoxidation and antioxidation of the body (54). SOD destroys superoxide radicals by dismutase to produce hydrogen peroxide, which is continuously reduced by catalase or GSH-PX activity (55). Thus, SOD and GSH-PX are able to protect cells from injury. When ferroptosis occurs in the organism, SLC7A11 expression on the cell membrane is suppressed (56), and cells then take up less cysteine. GSH is continuously consumed and synthesis cannot continue. Consequently, the synthesis of GPX4 is blocked, which disrupts the ability of the cell to scavenge reactive oxygen species (ROS), leading to ROS accumulation and triggering ferroptosis (57). It has been found that persistent inflammation and oxidative stress are important mediators of cancer development and progression (58). In the present study, the accumulation of excess lipid peroxides induced by iron overload activated ferroptosis in the pancreas. Ferroptosis has been reported to be involved in numerous pathological processes, including neurotoxicity (59), acute renal failure (60), hepatotoxicity (61) and pancreatic cancer (43). Studies have confirmed a key role for ferroptosis in AP, and addition of the ferroptosis inhibitor liproxstatin-1 or upregulation of GPX4 slowed AP and acute kidney injury in rats (62,63). These findings illustrate the possibility that the iron overload-induced ferroptosis in this experimental model leads to spontaneous formation of CP in mice, resulting in pancreatic acinar cell death and dysfunction. However, further validation is required to reach this conclusion. Meanwhile, ferroptosis may become a new target for the study of pancreatitis, and provide a new idea for the clinical research of pancreatitis. However, little is known about the exact mechanism of how iron overload affects the progression of pancreatitis, and further studies of the interaction between iron and pancreatic function are also needed to clarify the role of iron in the pancreas.

In summary, the present study provides evidence that secondary iron overload induced by multiple intraperitoneal injections of iron dextran resulted in massive iron deposition in the pancreas of mice. Iron-overloaded mice developed CP with elevated levels of serum amylase and lipase, upregulated gene expression of pro-inflammatory factors and increased infiltration of immune cells (Fig. 6). Moreover, iron overload also led to pancreatic fibrosis, oxidative stress and ferroptosis. This study suggests that secondary iron overload is a risk factor for pancreatitis and highlights the importance of iron in maintaining the normal functions of the pancreas.

Acknowledgements

Not applicable.

Funding

This study was supported by the Natural Science Foundation of Zhejiang Province of China (grant no. LZ20C170004), the National Natural Science Foundation of China (grant no. 31872363), the 'Ten Thousand Plan' Innovation Leader of Zhejiang Province of China (grant no. 2020R52007) and the Fundamental Research Funds for the Central Universities (grant no. 226-2022-00023).

Availability of data and materials

The datasets used and/or analyzed during the current study are available from the corresponding author on reasonable request.

Authors' contributions

CT, JZ and QX performed the experiments. CT, HY and HD analyzed the data. JZ conducted the literature search and analyzed the data. HY and HD designed the study and confirm the authenticity of all the raw data. All authors read and approved the final manuscript.

Ethics approval and consent to participate

All experiments were reviewed and approved by the Committee of Laboratory Animal Care and Animal Research Ethics Committee of Zhejiang University (approval no. 20077).

Patient consent for publication

Not applicable.

Competing interests

The authors declare that they have no competing interests.

References

1. Sarkar J, Potdar AA and Saidel GM: Whole-body iron transport and metabolism: Mechanistic, multi-scale model to improve treatment of anemia in chronic kidney disease. PLoS Comput Biol 14: e1006060, 2018.
2. Puig S, Ramos-Alonso L, Romero AM and Martinez-Pastor MT: The elemental role of iron in DNA synthesis and repair. Metallomics 9: 1483-1500, 2017.
3. Ganz T and Nemeth E: Iron homeostasis in host defence and inflammation. Nat Rev Immunol 15: 500-510, 2015.
4. Hentze MW, Muckenthaler MU, Galy B and Camaschella C: Two to tango: Regulation of mammalian iron metabolism. Cell 142: 24-38, 2010.
5. Ganz T: Systemic iron homeostasis. Physiol Rev 93: 1721-1741, 2013.
6. Fernandez RJM, Moreno-Navarrete JM and Manco M: Iron influences on the Gut-Brain axis and development of type 2 diabetes. Crit Rev Food Sci Nutr 59: 443-449, 2019.
7. Zafon C, Lecube A and Simo R: Iron in obesity. An ancient micronutrient for a modern disease. Obes Rev 11: 322-328, 2010.
8. Mayneris-Perxachs J, Cardellini M, Hoyles L, Latorre J, Davato F, Moreno-Navarrete JM, Arnoriaga-Rodriguez M, Serino M, Abbott J, Barton RH, *et al*: Iron status influences non-alcoholic fatty liver disease in obesity through the gut microbiome. Microbiome 9: 104, 2021.
9. Xu S: Iron and atherosclerosis: The link revisited. Trends Mol Med 25: 659-661, 2019.
10. Fleming RE and Ponka P: Iron overload in human disease. N Engl J Med 366: 348-359, 2012.
11. Fernandez-Real JM and Manco M: Effects of iron overload on chronic metabolic diseases. Lancet Diabetes Endocrinol 2: 513-526, 2014.
12. Brissot P, Pietrangelo A, Adams PC, de Graaff B, McLaren CE and Loréal O: Haemochromatosis. Nat Rev Dis Primers 4: 18016, 2018.
13. Bottomley SS: Secondary iron overload disorders. Semin Hematol 35: 77-86, 1998.
14. Che J, Yang J, Zhao B, Zhang G, Wang L, Peng S and Shang P: The effect of abnormal iron metabolism on osteoporosis. Biol Trace Elem Res 195: 353-365, 2020.
15. Hatunic M, Finucane FM, Brennan AM, Norris S, Pacini G and Nolan JJ: Effect of iron overload on glucose metabolism in patients with hereditary hemochromatosis. Metabolism 59: 380-384, 2010.
16. Roggero S, Quarello P, Vinciguerra T, Longo F, Piga A and Ramenghi U: Severe iron overload in blackfan-diamond anemia: A case-control study. Am J Hematol 84: 729-732, 2009.
17. Vogiatzi MG, Macklin EA, Trachtenberg FL, Fung EB, Cheung AM, Vichinsky E, Olivieri N, Kirby M, Kwiatkowski JL, Cunningham M, *et al*: Differences in the prevalence of growth, endocrine and vitamin D abnormalities among the various thalassaemia syndromes in North America. Br J Haematol 146: 546-556, 2009.
18. Berdoukas V, Nord A, Carson S, Puliyel M, Hofstra T, Wood J and Coates TD: Tissue iron evaluation in chronically transfused children shows significant levels of iron loading at a very young age. Am J Hematol 88: E283-E285, 2013.
19. Lee PJ and Papachristou GI: New insights into acute pancreatitis. Nat Rev Gastroenterol Hepatol 16: 479-496, 2019.
20. Lugea A, Waldron RT, Mareninova OA, Shalbueva N, Deng N, Su HY, Thomas DD, Jones EK, Messenger SW, Yang J, *et al*: Human pancreatic acinar cells: Proteomic characterization, physiologic responses, and organellar disorders in ex vivo pancreatitis. Am J Pathol 187: 2726-2743, 2017.
21. Singh VK, Yadav D and Garg PK: Diagnosis and management of chronic pancreatitis: A review: JAMA 322: 2422-2434, 2019.
22. Whitcomb DC, Frulloni L, Garg P, Greer JB, Schneider A, Yadav D and Shimosegawa T: Chronic pancreatitis: An international draft consensus proposal for a new mechanistic definition. Pancreatology 16: 218-224, 2016.
23. Kimita W and Petrov MS: Iron metabolism and the exocrine pancreas. Clin Chim Acta 511: 167-176, 2020.
24. Lunova M, Schwarz P, Nuraldeen R, Levada K, Kuscuoglu D, Stützle M, Spasić MV, Haybaeck J, Ruchala P, Jirsa M, *et al*: Hepcidin knockout mice spontaneously develop chronic pancreatitis owing to cytoplasmic iron overload in acinar cells. J Pathol 241: 104-114, 2017.
25. Pauk M, Kufner V, Rumenovic V, Dumic-Cule I, Farkas V, Milosevic M, Bordukalo-Niksic T and Vukicevic S: Iron overload in aging Bmp6(/) mice induces exocrine pancreatic injury and fibrosis due to acinar cell loss. Int J Mol Med 47: 60, 2021.
26. Pelucchi S, Ravasi G and Piperno A: Ceruloplasmin variants might have different effects in different iron overload disorders. J Hepatol 75: 1003-1004, 2021.
27. Ganz T: Hepcidin and iron regulation, 10 years later. Blood 117: 4425-4433, 2011.
28. Yildirim M, Kaplan M, Duzenli T, Tanoglu A, Kucukodaci Z, Tastan YO, Guney BC and Serindag Z: Pentoxifylline has favorable preventive effects on experimental chronic pancreatitis model. Scand J Gastroenterol 55: 236-241, 2020.
29. Livak KJ and Schmittgen TD: Analysis of relative gene expression data using real-time quantitative PCR and the 2(-Delta Delta C(T)) method. Methods 25: 402-408, 2001.
30. Ma W, Jia L, Xiong Q and Du H: Iron overload protects from obesity by ferroptosis. Foods 10: 1787, 2021.
31. Xiong H, Zhang C, Han L, Xu T, Saeed K, Han J, Liu J, Klaassen CD, Gonzalez FJ, Lu Y and Zhang Y: Suppressed farnesoid X receptor by iron overload in mice and humans potentiates iron-induced hepatotoxicity. Hepatology 76: 387-403, 2021.
32. Zhang DL, Hughes RM, Ollivierre-Wilson H, Ghosh MC and Rouault TA: A ferroportin transcript that lacks an iron-responsive element enables duodenal and erythroid precursor cells to evade translational repression. Cell Metab 9: 461-473, 2009.
33. Petrillo S, Manco M, Altruda F, Fagoonee S and Tolosano E: Liver sinusoidal endothelial cells at the crossroad of iron overload and liver fibrosis. Antioxid Redox Signal 35: 474-486, 2021.

34. Martin D, Nay K, Robin F, Rebillard A, Orfila L, Martin B, Leroyer P, Guggenbuhl P, Dufresne S, Noirez P, *et al*: Oxidative and glycolytic skeletal muscles deploy protective mechanisms to avoid atrophy under pathophysiological iron overload. J Cachexia Sarcopenia Muscle 13: 1250-1261, 2022.
35. Lohr JM, Dominguez-Munoz E, Rosendahl J, Besselink M, Mayerle J, Lerch MM, Haas S, Akisik F, Kartalis N, Iglesias-Garcia J, *et al*: United European gastroenterology evidence-based guidelines for the diagnosis and therapy of chronic pancreatitis (HaPanEU). United European Gastroenterol J 5: 153-199, 2017.
36. Beyer G, Habtezion A, Werner J, Lerch MM and Mayerle J: Chronic pancreatitis. Lancet 396: 499-512, 2020.
37. Kleeff J, Whitcomb DC, Shimosegawa T, Esposito I, Lerch MM, Gress T, Mayerle J, Drewes AM, Rebours V, Akisik F, *et al*: Chronic pancreatitis. Nat Rev Dis Primers 3: 17060, 2017.
38. Manohar M, Verma AK, Venkateshaiah SU, Sanders NL and Mishra A: Pathogenic mechanisms of pancreatitis. World J Gastrointest Pharmacol Ther 8: 10-25, 2017.
39. Xue J, Sharma V and Habtezion A: Immune cells and immune-based therapy in pancreatitis. Immunol Res 58: 378-386, 2014.
40. Kolaczkowska E and Kubes P: Neutrophil recruitment and function in health and inflammation. Nat Rev Immunol 13: 159-175, 2013.
41. Grunwald B, Harant V, Schaten S, Fruhschutz M, Spallek R, Hochst B, Stutzer K, Berchtold S, Erkan M, Prokopchuk O, *et al*: Pancreatic premalignant lesions secrete tissue inhibitor of metalloproteinases-1, which activates hepatic stellate cells via CD63 signaling to create a premetastatic niche in the liver. Gastroenterology 151: 1011-1024.e1017, 2016.
42. Chin AC and Parkos CA: Neutrophil transepithelial migration and epithelial barrier function in IBD: potential targets for inhibiting neutrophil trafficking. Ann N Y Acad Sci 1072: 276-287, 2006.
43. Dai E, Han L, Liu J, Xie Y, Zeh HJ, Kang R, Bai L and Tang D: Ferroptotic damage promotes pancreatic tumorigenesis through a TMEM173/STING -dependent DNA sensor pathway. Nat Commun 11: 6339, 2020.
44. Han L, Ma J, Duan W, Zhang L, Yu S, Xu Q, Lei J, Li X, Wang Z, Wu Z, *et al*: Pancreatic stellate cells contribute pancreatic cancer pain via activation of sHH signaling pathway. Oncotarget 7: 18146-18158, 2016.
45. Kirkegård J, Mortensen FV and Cronin-Fenton D: Chronic pancreatitis and pancreatic cancer risk: A systematic review and meta-analysis. Am J Gastroenterol 112: 1366-1372, 2017.
46. Chen B, Li J, Fellows GF, Sun Z and Wang R: Maintaining human fetal pancreatic stellate cell function and proliferation require beta1 integrin and collagen I matrix interactions. Oncotarget 6: 14045-14059, 2015.
47. Tang D and Kroemer G: Ferroptosis. Curr Biol 30: R1292-R1297, 2020.
48. Dixon SJ, Lemberg KM, Lamprecht MR, Skouta R, Zaitsev EM, Gleason CE, Patel DN, Bauer AJ, Cantley AM, Yang WS, *et al*: Ferroptosis: An iron-dependent form of nonapoptotic cell death. Cell 149: 1060-1072, 2012.
49. Xie Y, Hou W, Song X, Yu Y, Huang J, Sun X, Kang R and Tang D: Ferroptosis: Process and function. Cell Death Differ 23: 369-379, 2016.
50. Wang C, Zheng L, Liu S, Guo X, Qu Y, Gao M, Cui X and Yang Y: A novel acidic polysaccharide from the residue of Panax notoginseng and its hepatoprotective effect on alcoholic liver damage in mice. Int J Biol Macromol 149: 1084-1097, 2020.
51. Ayala A, Muñoz MF and Argüelles S: Lipid peroxidation: Production, metabolism, and signaling mechanisms of malondialdehyde and 4-hydroxy-2-nonenal. Oxid Med Cell Longev 2014: 360438, 2014.
52. Jové M, Mota-Martorell N, Pradas I, Martín-Gari M, Ayala V and Pamplona R: The advanced lipoxidation end-product malondialdehyde-lysine in aging and longevity. Antioxidants (Basel) 9: 1132, 2020.
53. Tsikas D: Assessment of lipid peroxidation by measuring malondialdehyde (MDA) and relatives in biological samples: Analytical and biological challenges. Anal Biochem 524: 13-30, 2017.
54. Olsvik PA, Kristensen T, Waagbø R, Rosseland BO, Tollefsen KE, Baeverfjord G and Berntssen MHG: MRNA expression of antioxidant enzymes (SOD, CAT and GSH-Px) and lipid peroxidative stress in liver of Atlantic salmon (Salmo salar) exposed to hyperoxic water during smoltification. Comp Biochem Physiol C Toxicol Pharmaco 141: 314-323, 2005.
55. Sefi M, Fetoui H, Lachkar N, Tahraoui A, Lyoussi B, Boudawara T and Zeghal N: Centaurium erythrea (Gentianaceae) leaf extract alleviates streptozotocin-induced oxidative stress and β-cell damage in rat pancreas. J Ethnopharmacol 135: 243-250, 2011.
56. Dolma S, Lessnick SL, Hahn WC and Stockwell BR: Identification of genotype-selective antitumor agents using synthetic lethal chemical screening in engineered human tumor cells. Cancer Cell 3: 285-296, 2003.
57. Forcina GC and Dixon SJ: GPX4 at the crossroads of lipid homeostasis and ferroptosis. Proteomics 19: e1800311, 2019.
58. Yao W, Qiu HM, Cheong KL and Zhong S: Advances in anti-cancer effects and underlying mechanisms of marine algae polysaccharides. Int J Biol Macromol 221: 472-485, 2002.
59. Xia Y, Sun X, Luo Y and Stary CM: Ferroptosis contributes to isoflurane neurotoxicity. Front Mol Neurosci 11: 486, 2018.
60. Belavgeni A, Meyer C, Stumpf J, Hugo C and Linkermann A: Ferroptosis and necroptosis in the kidney. Cell Chem Biol 27: 448-462, 2020.
61. Yamada N, Karasawa T, Kimura H, Watanabe S, Komada T, Kamata R, Sampilvanjil A, Ito J, Nakagawa K, Kuwata H, *et al*: Ferroptosis driven by radical oxidation of n-6 polyunsaturated fatty acids mediates acetaminophen-induced acute liver failure. Cell Death Dis 11: 144, 2020.
62. Fan R, Sui J, Dong X, Jing B and Gao Z: Wedelolactone alleviates acute pancreatitis and associated lung injury via GPX4 mediated suppression of pyroptosis and ferroptosis. Free Radic Biol Med 173: 29-40, 2021.
63. Ma D, Li C, Jiang P, Jiang Y, Wang J and Zhang D: Inhibition of ferroptosis attenuates acute kidney injury in rats with severe acute pancreatitis. Dig Dis Sci 66: 483-492, 2021.